Defence Science Journal, Vol. 61, No. 4, July 2011, pp. 364-369, DOI: 10.14429/dsj.61.1089

SHORT COMMUNICATION

Viscous Shock Layer Method to Predict Communication Blackout during Re-entry Phase

Rhea George and R.K. Gupta

Advanced Systems Laboratory, Kanchanbagh, Hyderabad- 500 058
E-mail: rheageorge@gmail.com and rkg_204@yahoo.co.in

ABSTRACT

Communication blackout generally occurs during the re-entry at high velocities through the atmosphere. Air ahead of the re-entry vehicle dissociates and then ionises, leading to the production of electrons. These electrons may reflect or attenuate the communication signals. Electron densities with plasma frequency exceeding the communication frequency lead to blackout. Electron density is a function of the body shape, velocity and altitude. The viscous shock layer method is used to predict the electron density, and thereby the plasma frequency for various configurations. This method is successfully implemented for analytic and non-analytic geometry configurations available in the literature. The electron densities computed for the RAM-C configuration agree well with the flight results. The onset of blackout during the re-entry phase is also predicted reasonably well by this method. The method performs well at high altitudes, where nonequilibrium conditions prevail.

Keywords: Communication blackout, hypersonic, re-entry, plasma, viscous shock layer method, plasma frequency, Communication frequency

NOMENCLATURE

C_i	Concentration of species i, ρ_i/ρ
C_p	Specific heat at constant pressure
e	Electronic charge
f_p	Plasma frequency
FVSL	Fully viscous shock layer
k_{b_r}	Backward reaction rate constant
k_{f_r}	Forward reaction rate constant
m	Mass of electron
M_1, M_2, M_3	Catalytic third bodies
nj	Number of species plus catalytic third bodies
nr	Number of chemical reactions
N_e	Electron density
P	Pressure, $p^*/(\rho^* u_\infty^{*2})$
r	Body radius, r^*/R_n^*
R_n^*	Body nose radius
s	Coordinate measured along body surface, s^*/R_n^*
T	Temperature, T^*/T_{ref}^*
T_{ref}^*	Reference temperature, $u_\infty^{*2}/C_{p\infty}^*$
TVSL	Thin viscous shock layer
u	Velocity component tangent to body surface, u^*/u_∞^*
u_∞^*	Free stream velocity
v	Velocity component normal to body surface, v^*/u_∞^*
X_i	Chemical species and catalytic third bodies
y	Coordinate measured normal to the body, y^*/R_n^*
z	Coordinate measured along body axis, z^*/R_n^*

Greek Symbols

α_{ri}	Forward stoichiometric coefficient
β_{ri}	Backward stoichiometric coefficient
ε	Permittivity of vaccum
ρ	Density, ρ^*/ρ_∞^*

Superscripts/Subscripts

*	Indicator for dimensional quantities
i	Species i
sh	Value behind the shock
w	Wall value
∞	Free stream value

1. INTRODUCTION

Communication blackout generally occurs during re-entry at high velocities through the atmosphere. The ionised gas forms a layer of plasma over the re-entry vehicle. The frequency of oscillation of the electrons about their mean position is called plasma frequency. If the plasma frequency exceeds the communication frequency, it attenuates the communication signal, leading to communication blackout.

The plasma frequency, f_p in Hz is obtained from Eqn (1), where N_e is the electron density per cc, e is the electronic charge, ε the permittivity of vacuum, and m is the mass of electron.

Received 23 March 2011, published online 25 July 2011

$$f_p = \frac{1}{2\pi}\sqrt{\frac{N_e.e^2}{\varepsilon.m}} \approx 9000\sqrt{N_e} \quad (1)$$

Viscous shock layer (VSL) approach is one of the methods to estimate the electron density in the shock layer. Communication is restored at lower altitudes due to reduction in vehicle velocity and increase in collision frequency of electrons with neutral particles in high density air.

At atmospheric pressure, dissociation of oxygen and nitrogen molecules start at 2000 K and 4000 K, respectively. Molecular oxygen is completely dissociated at 4000 K. Molecular nitrogen is totally dissociated at 9000 K. Above these temperatures, the gas becomes a partially ionised plasma consisting of *O, O*$^+$*, N, N*$^+$ and electrons[1]. In the temperature range of 4000 K to 6000 K, small amount of *NO* is formed, some of which ionise to form *NO*$^+$ and electrons. The electron density due to *NO* ionisation may be sufficient to cause communication blackout. The mechanism by which free electrons in the plasma affect the electromagnetic wave signals has been explained in literature[2].

Viscous shock layer approach can be used to compute viscous, hypersonic flows over blunt bodies. The entire flow-field, from the body to the shock, is treated in a combined manner. One of the pioneers in the development of viscous shock layer method was Davis[3]. The VSL equations hold across the entire shock layer, and hence are more powerful than the boundary layer equations[1]. These equations are parabolic, and hence, a downstream marching solution can be obtained using finite difference method. The perfect gas viscous shock layer method of Davis was extended for chemically reacting nonequilibrium flow[4] and for nonanalytic blunt bodies with multi-component, ionising air or dissociated oxygen[5].

The VSL code described here was developed[6] to predict hypersonic, low Reynolds number flows over nonanalytic blunt bodies. The first nonequilibrium gas chemistry model is for dissociating oxygen and the second is for ionising, multi-component air. The aim of this study is to implement the VSL code, named Viscous Shock Layer-Advanced Systems Laboratory (VSLASL) for different nonanalytic blunt bodies like the 20° blunted cone, radio attenuation measurements-C (RAM-C) and space capsule recovery experiment (SRE) configurations to predict the electron density.

2. GOVERNING EQUATIONS

The governing equations include the continuity equation, *s*-momentum equation, *y*-momentum, energy equation, species conservation equation in addition to the equation of state. Since these equations are given in literature[3, 4] these are not presented here. The *y*-momentum equation is solved in the first iteration assuming thin viscous shock layer (TVSL) and subsequent iterations use either TVSL or fully viscous shock layer (FVSL). The VSL equations are second order accurate in the Reynolds number parameter.

The independent and dependent variables were normalised by their local shock values to transform the shock-layer equations. Solutions of continuity and *y*-momentum equations were obtained by integration with the trapezoidal rule. The transformed equations for the remaining governing equations were expressed in the standard form of a parabolic partial differential equation. Finite difference method[3] was used for solving the governing equations.

3. THERMODYNAMIC AND TRANSPORT PROPERTIES

Species enthalpy and specific heat were computed by second-order Lagrangian interpolation from the tables included in the program. The viscosity of each individual species was calculated by curve fit relations in the program. The mixture viscosity and thermal conductivity were evaluated using semi-empirical relations.

4. BOUNDARY CONDITIONS

At the body, no-slip boundary conditions were specified. The species concentrations in the free stream were specified as C_O =0, C_N = 0, C_{O_2} = 0.23456, C_{NO} = 0, C_{NO^+} = 0, C_{N_2} = 0.76544.

A fully catalytic wall leads to recombination of all atoms at the wall. The recombination reactions release heat and increase the heating of the surface. If the surface is non-catalytic, the recombination does not take place and heating of the surface is relatively low[7].

5. CHEMICAL REACTION MODEL

The chemical reactions are assumed to proceed at a finite rate. The chemical reaction equations are written in the general stoichiometric form as in Eqn. (2), where r = 1,2,... nr (nr = number of reactions) and nj is equal to sum of the number of species and catalytic third bodies. X_i represents the chemical species and catalytic third bodies, and α_{ri} and β_{ri} are the stoichiometric coefficients for reactants and products. The reaction rate constants, k_{f_r} and k_{b_r} are the forward and backward reaction rate constants.

$$\sum_{i=1}^{nj} \alpha_{ri} X_i \underset{k_{br}}{\overset{k_{fr}}{\leftrightarrow}} \sum_{i=1}^{nj} \beta_{ri} X_i \quad (2)$$

The reactions used for dissociating oxygen are given by Eqns (3) and (4) as

$$O_2 + O_2 \leftrightarrow O + O + O_2 \quad (3)$$

$$O_2 + O \leftrightarrow O + O + O \quad (4)$$

For multi-component air, the reactions and chemical reaction rates have been taken from literature[8]. The seven reactions for the seven species (O_2, N_2, *NO, O, N,* NO^+ and e^-) are given in Eqn. (5) through Eqn. (11) where M_1, M_2 and M_3 are the catalysts.

$$O_2 + M_1 \leftrightarrow O + O + M_1 \quad (5)$$

$$N_2 + M_2 \leftrightarrow N + N + M_2 \quad (6)$$

$$N_2 + N \leftrightarrow N + N + N \quad (7)$$

$$NO + M_3 \leftrightarrow N + O + M_3 \quad (8)$$

$$NO + O \leftrightarrow O_2 + N \quad (9)$$

$$N_2 + O \leftrightarrow NO + N \quad (10)$$

$$N + O \leftrightarrow NO^+ + e^- \quad (11)$$

6. DESCRIPTION OF VSL PROGRAMME

The VSL programme is written in Fortran. This programme is applicable to nonanalytic blunt bodies in addition to analytic bodies like the paraboloid and hyperboloid. The first global iteration is for TVSL only. Subsequent global iterations may be for TVSL or FVSL. The altitude and body nose radius, free stream density, body wall temperature, free stream temperature and free stream velocity were specified. At each stream-wise '*s*' location, the shock-layer equations are solved in the order of species, energy, *s*-momentum, continuity, and *y*-momentum. For spherically blunted cones, the pressure distribution being highly non-Newtonian, an initial shock shape was input to the program.

7. LIMITATIONS

The limitations of VSL method are as follows:

(i) The VSL method, being a space-marching scheme, cannot be applied to separated flows.

(ii) For solving flow past a spherically blunted cone, the discontinuity in surface curvature at the sphere-cone tangent point creates difficulties in solving the equations in a stable manner.

(iii) For conditions approaching equilibrium, there is increased difficulty in obtaining a converged solution at the stagnation point.

8. RESULTS

The present VSL code is run for both analytic and nonanalytic bodies. The implementation of this code is checked by running it for the sample cases[6]. On successful implementation of these sample cases, the code is examined for spherically-blunted cones such as 20° blunted cone, RAM-C 9° blunted cone and SRE configurations.

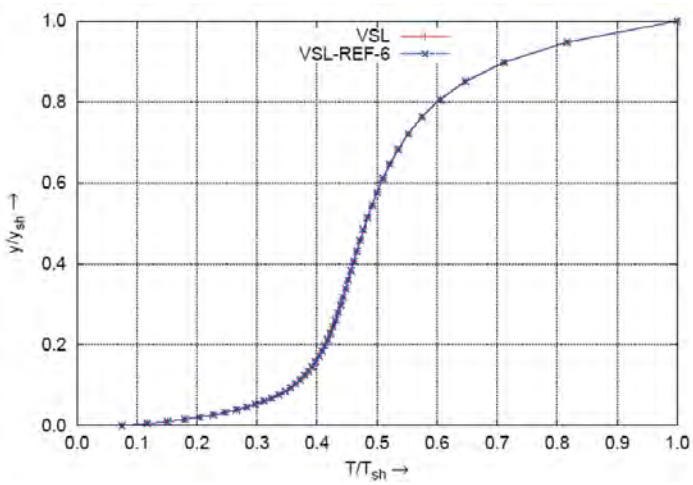

Figure 1. Temperature profile over hyperboloid in stagnation region.

8.1 Sample Cases

8.1.1 Hyperboloid

The first analytic geometry considered is the 31° hyperboloid sample case[6] at an altitude of 74.6 km with a free stream velocity of 7.6 km/s. The temperature profile in the stagnation region, with the maximum temperature at the shock, is shown in Fig. 1. The results obtained match perfectly with results available in the literature[6].

8.1.2 140B Orbiter

The second sample geometry considered is the 140B Orbiter, for which the geometry is specified in a tabular form. The electron density at the stagnation point of this body matches extremely well with value of electron density as available with literature[6] as shown in Fig. 2. It is observed from this figure that the peak electron density occurs within the shock layer. Since the sample cases are implemented successfully, the VSL code is extended to spherically-blunted cones.

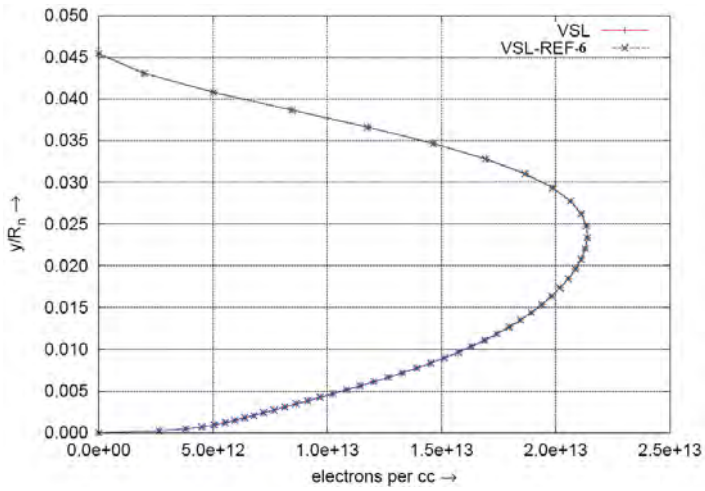

Figure 2. Electron density over 140B Orbiter at stagnation point.

8.2 Spherically-blunted Cone Geometries

8.2.1 20° Blunted Cone

The blunted cone geometry considered[9] is a cone of 20° half angle with a nose radius of 38.1 mm. The nondimensional pressure on the body wall in the nose region is compared with literature[9] and plotted in Fig. 3. The pressure drop due to expansion of the flow over the spherical portion and almost constant pressure over the conical portion is clearly observed from the above figure. The nondimensional temperature at the stagnation point extending from the body to the shock is shown in Fig. 4. The mass fraction of various species in the stagnation region is compared in Fig. 5. It is observed that the mass fraction profiles match reasonably well with the the mass fraction profiles available in the literature[9]. The small variations in the mass fraction profiles might be due to differences in the thermodynamic properties. The degree of nonequilibrium in the flow field is evident from the mass fraction profiles.

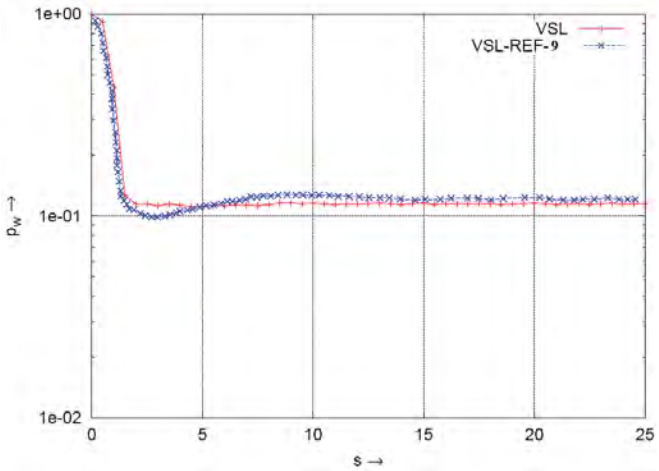

Figure 3. Body pressure comparison over 20° sphere-cone in the nose region.

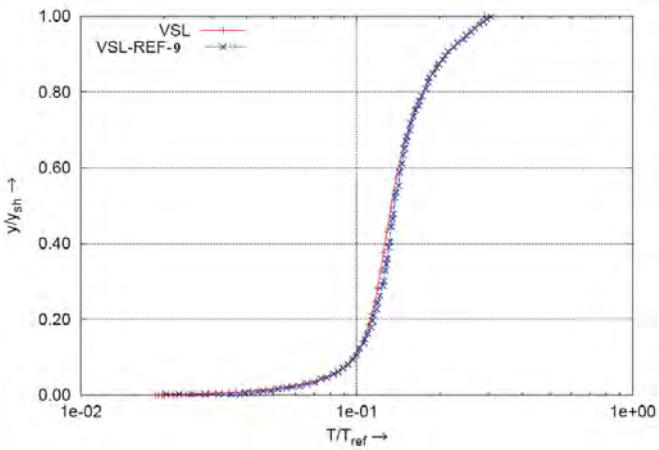

Figure 4. Temperature profile comparison in the stagnation region of 20° sphere-cone.

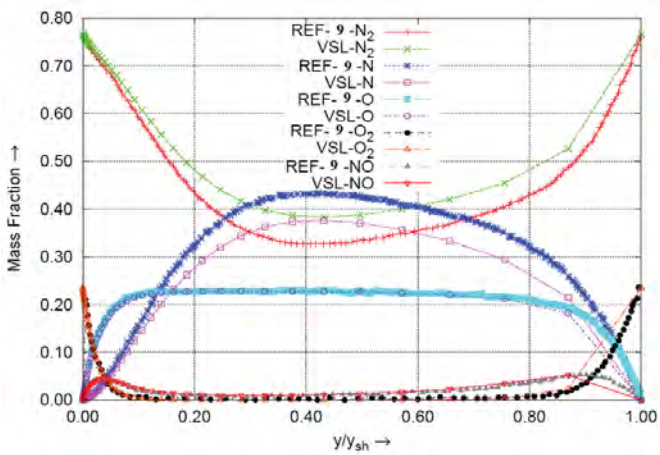

Figure 5. Mass fraction comparison over 20° sphere-cone (stagnation region, $s = 0$).

8.2.2 RAM-Series C-9° Blunted Cone

The radio attenuation measurements (RAM) project consisted of spherically-blunted cones used to study the plasma characteristics during re-entry[10]. The RAM-series C consists of flight experiments in a higher velocity regime (about 7.6 km/s)[11]. The RAM-Series C configuration consists of a 9° cone with a bluntness radius of 152.4 mm.

The change in curvature at the sphere-cone junction of the RAM-Series C geometry causes problems in obtaining the shock shape properly. Hence the shock shape computed from a code based on inviscid shock layer[12] is given as an input to the viscous shock layer code. This helps in better resolution of the shock shape. The runs are carried out assuming no shock slip as in the literature[5]. The electron density at the antenna location for altitudes varying from 61 to 76 km computed from the present code are compared with literature[5, 13]. As shown in Fig. 6, the order of the electron density at the antenna location obtained from this code matches fairly well with what is available in the literature. It is observed from the above figure that with decrease in altitude, the electron density increases.

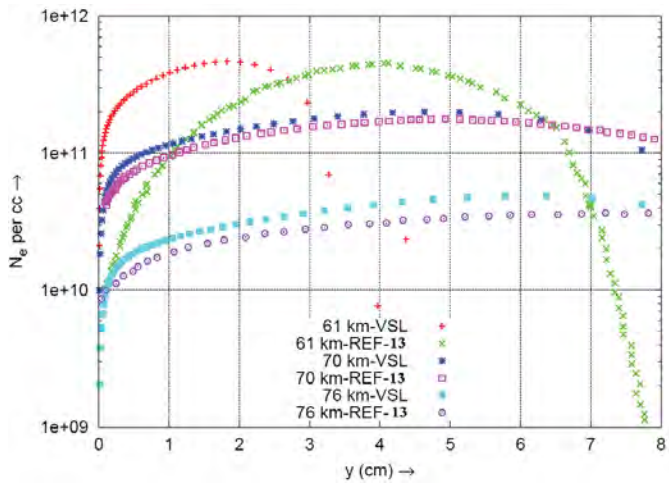

Figure 6. Electron density profiles at various altitudes for RAM-Series C.

The shock layer thickness at an altitude of 70 km compares reasonably well with what is available in the literature[5] as shown in Fig. 7. The temperature profile at the antenna location obtained from the present code also compares well with what is available in the literature[5] for the same altitude as shown in Fig. 8. It is observed from the above plot that the maximum temperature occurs within the shock layer. The temperature distribution behind the shock at 70 km altitude also matches well with what is available in the literature as presented in Fig. 9. As expected, the temperature behind the shock decreases along the surface as the shock strength reduces downstream of the stagnation point.

8.2.3 SRE Configuration

The SRE configuration consists of a blunted double cone. The bluntness radius is 508.8 mm while the cone angles are 20° and 25°. Since the antenna is located on the 20° cone, only this part was considered as the SRE geometry in the present VSLASL code. The walls were assumed to be catalytic and at a temperature of 1000 K as in the VSL results reported in the literature[14]. Shock slip boundary condition was applied to enable comparison with literature. The electron densities at

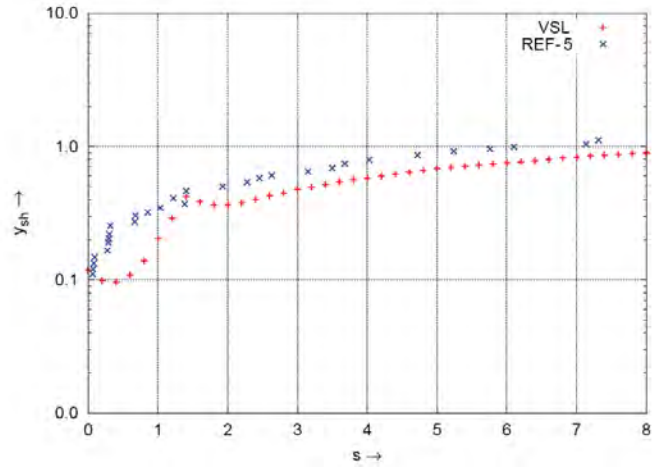

Figure 7. Shock layer thickness distribution at 70 km for RAM-Series C.

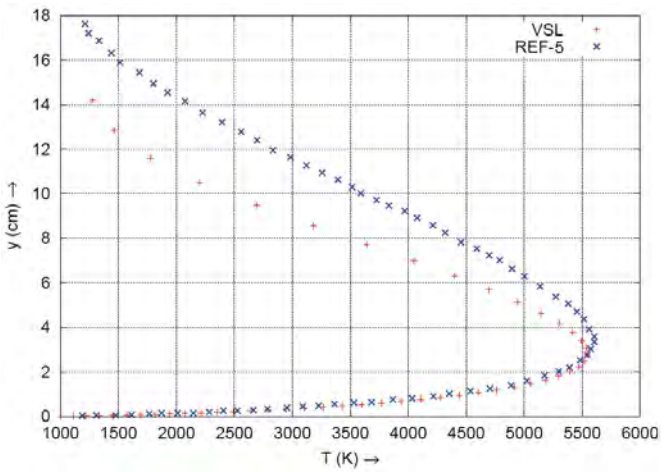

Figure 8. Temperature profile at antenna location for RAM-Series C at an altitude of 70 km.

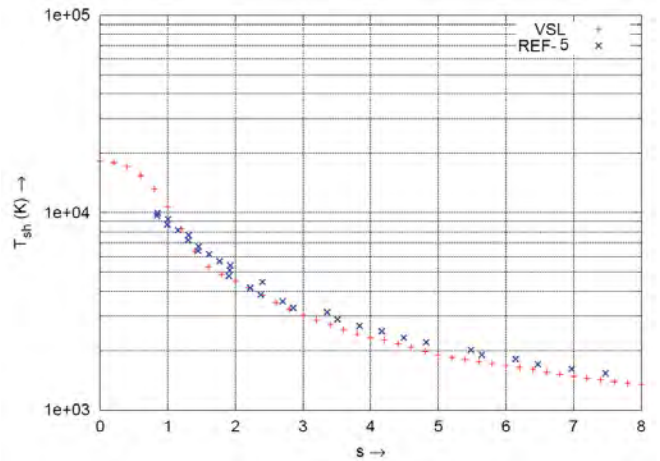

Figure 9. Shock temperature distribution for RAM-Series C at an altitude of 70 km.

the stagnation and antenna location at an altitude of 80 km are plotted in Fig. 10. The viscous shock layer code is able to predict the electron density levels quite well as compared with the literature[14]. The maximum electron densities along the axial direction for 80 km and 85 km are shown in Fig.11. A fairly good match is obtained in predicting the maximum

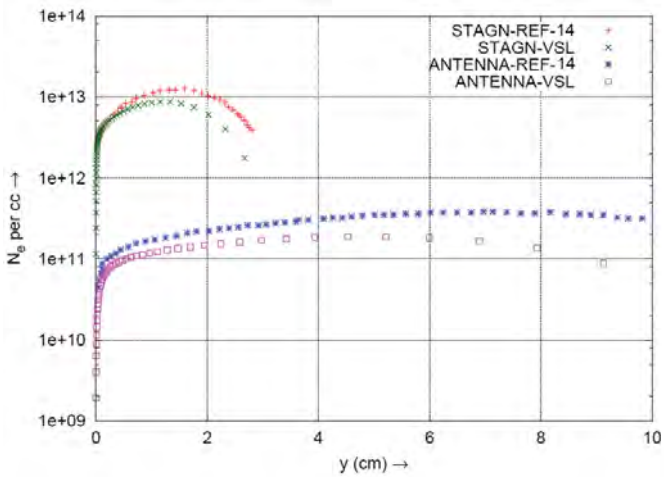

Figure 10. Electron density over SRE configuration at an altitude of 80 km.

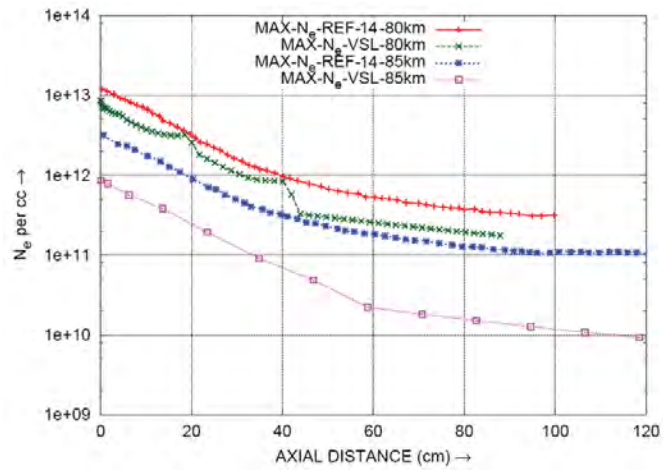

Figure 11. Maximum electron density along the axis for 80 km and 85 km altitudes.

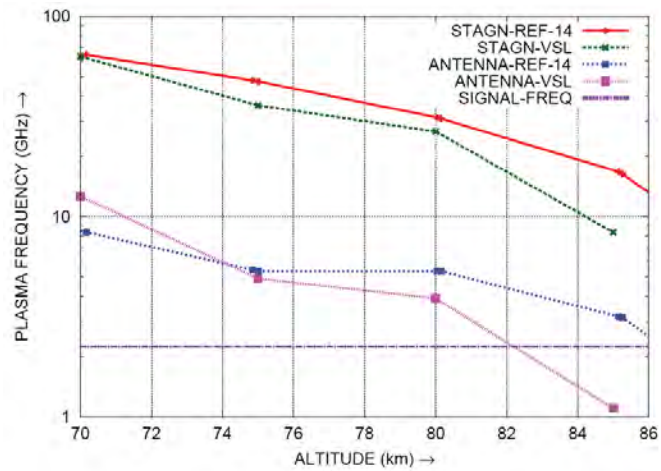

Figure 12. Plasma frequencies at various altitudes for SRE configuration.

electron density level. The kinks in the plot could be due to the change in curvature near the sphere-cone junction. The plasma frequency, obtained from the electron density, at altitudes varying from 70 km to 85 km at the stagnation and antenna locations are plotted in Fig. 12. The communication signal frequency is 2.25 GHz. The present code predicts the onset of blackout to be at about 82 km which matches very well with flight, where the onset of blackout was at 81 km[14].

9. CONCLUSIONS

The present Viscous Shock Layer-Advanced Systems Laboratory is implemented for both analytic and nonanalytic body geometries. The results from the present code for spherically-blunted cones like the 20° cone, RAM-Series C and SRE configurations compare favourably with available literature. Various parameters such as the temperature, pressure, species mass fraction, electron density, and plasma frequency are found to match well with literature. A good comparison is obtained between the electron densities for the RAM-Series C configuration predicted by the present code and the measured flight electron densities. Hence, the present code can be used to compute the electron densities for similar spherically blunted cones. Since this code is meant for nonequilibrium flows, it functions well at higher altitudes. But convergence problems arise at lower altitudes, which aid in achieving the equilibrium state. Consequently this code can be used to compute the electron density over bodies during re-entry phase and predict the altitude corresponding to the onset of communication blackout.

ACKNOWLEDGEMENTS

The authors thank Shri Avinash Chander, Director, Advanced Systems Laboratory (ASL), Hyderabad, for granting permission to publish this work. The efforts of Shri Rahul Chopde, formerly working at ASL is also gratefully acknowledged.

REFERENCES

1. Anderson, J.D. Hypersonic and high temperature gas dynamics. McGraw-Hill Series. 1989.
2. Rybak, J.P. & Churchill, R.J. Progress in re-entry communications. *IEEE Trans. Aero. Electro. Syst.*, 1971, **AES-7**(5), 879-94.
3. Davis, R.T. Numerical solution of the hypersonic viscous shock layer equations. *AIAA Journal*, 1970, **8**(5), 843-51.
4. Moss, J.N. Reacting viscous shock layer solutions with multicomponent diffusion and mass injection. NASA, USA. NASA Report No. NASA-TR-411, 1974.
5. Miner, E.W. & Lewis, C.H. Hypersonic ionising air viscous shock-layer flows over nonanalytic blunt bodies. NASA, USA. NASA Report No. NASA-CR-2550, 1975.
6. Miner, E.W. & Lewis, C.H. Computer user's guide for a chemically reacting viscous shock-layer program. NASA, USA. NASA Report No. NASA-CR-2551, 1975.
7. Bertin, J.J. Hypersonic aerothermodynamics. AIAA Education Series, 1994.
8. Blottner, F.G.; Johnson, M. & Ellis, M. Chemically reacting viscous flow programme for multi-component gas mixtures. Sandia Laboratories. Report No. SC-RR-70-754, 1971.
9. Cheatwood, F.M. & DeJarnette, F.R. An approximate viscous shock layer technique for calculating nonequilibrium hypersonic flows about blunt-nosed bodies. AIAA Paper No. AIAA 92-0498, 1992.
10. Weaver, W.L. & Bowen, J.T. Entry trajectory, entry environment and analysis of spacecraft motion for the RAM-Series C-III experiment. NASA, USA. NASA Report No. NASA-TMX-2562, 1972.
11. Widhopf, G.; Kaplan, B. & Jannone, J. Numerical flow field prediction for RAM-Series C. NASA, USA. NASA Report No. NASA-CR-66109, 1966.
12. Zoby, E. V. & Graves, R.A., Jr. A computer programme for calculating the perfect gas inviscid flow field about blunt axisymmetric bodies at an angle of attack of 0°. NASA, USA. NASA Report No. NASA-TMX-2843, 1973.
13. Swift, C.T.; Beck, F.B.; Thomson, J. and Castellow, S.L. Jr., RAM C-III S-Band diagnostic experiment. NASA, USA. NASA Report No. NASA-SP-252, 1970.
14. Asokarajan. N.; Ashok, V. & Mehta, R.C. Electron concentration study for SRE re-entry flight. Vikram Sarabhai Space centre, Thiruananthapuram, India, VSSC Report No. VSSC/ARD/TM/SRE/054/2007, 2007.

Contributors

Ms Rhea George received her BE (Mech Engg) from Osmania University in 2003 and MTech (Aerospace Engg) from IIT Madras, Chennai, in 2005. She is currently working as Scientist 'C' at Advanced Systems Laboratory(ASL), Hyderabad. Her areas of interest include external aerodynamics, hypersonic flows and aerothermodynamics.

Dr Rajesh Kumar Gupta obtained his ME(Aerospace Engg) from IISc, Bengaluru in 1984 and PhD from JNTU, Hyderabad in June 2011. Presently he is working as Technology Director at ASL, Hyderabad. His areas of interest are: Aerospace structures, vibration, composites, aerospace system configuration design.